



Full Text View

[Volume 31, Issue 8 \(August 2001\)](#)

Journal of Physical Oceanography

Article: pp. 2280–2296 | [Abstract](#) | [PDF \(654K\)](#)

Effects of Isopycnal and Diapycnal Mixing on the Stability of Oceanic Currents

Yves Morel

EPSHOM-CMO, Brest, France

James McWilliams

IGPP, University of California, Los Angeles, Los Angeles, California

(Manuscript received April 27, 2000, in final form November 8, 2000)

DOI: 10.1175/1520-0485(2001)031<2280:EOIADM>2.0.CO;2

ABSTRACT

This paper considers several influences of mixing on the stability of oceanic boundary currents, analyzed primarily in terms of the effects of mixing on the distribution of potential vorticity. This perspective relates both to the Charney–Stern criterion for the stability of currents and the Haynes–McIntyre constraints on the evolution of potential vorticity when mixing occurs. It is shown that diapycnal mixing can alter the structure of a stable current so that it becomes potentially unstable according to the Charney–Stern criterion. The effects of isopycnal diffusion and a viscous lateral boundary layer are also considered. Occurrences of instability are then illustrated with both computational solutions and experiments in a rotating tank. Finally, subsurface float trajectories are shown near the coast of Portugal that are suggestive of the instability of the boundary current downstream from the Mediterranean outflow, known to be subject to strong mixing.

1. Introduction

In this paper we investigate the formation of submesoscale vortices from intense coastal currents. For instance, gravity currents (with dense water flowing downhill) that originate from the exchange of water between two basins separated by a strait generate intense vortices in the interior of the ocean. A particular example of this is the meddies (Mediterranean Water eddies) generated from the subsurface Mediterranean outflow current along the Iberian coast.

Table of Contents:

- [Introduction](#)
- [Potential vorticity constraints](#)
- [Computational experiments](#)
- [Laboratory experiments](#)
- [Discussion](#)
- [REFERENCES](#)
- [APPENDIX](#)
- [TABLES](#)
- [FIGURES](#)

Options:

- [Create Reference](#)
- [Email this Article](#)
- [Add to MyArchive](#)
- [Search AMS Glossary](#)

Search CrossRef for:

- [Articles Citing This Article](#)

Search Google Scholar for:

- [Yves Morel](#)
- [James McWilliams](#)

This subject has been investigated previously. Among several proposed mechanisms, the one most frequently invoked is a mixed barotropic–baroclinic instability (see [Prater 1992](#); [Baey 1997](#)). This mechanism is known to have a necessary condition for the onset of instability, the Charney–Stern criterion, which states that the horizontal (or isopycnal) potential vorticity gradient must change sign somewhere within the flow. Potential vorticity (PV) is a tracer combining vorticity and density stratification that is conserved for each fluid particle in the absence of mixing. Therefore, when an oceanic basin exchanges its water adiabatically with another basin, the outflowing current often provides a source of distinctive PV values, depending on the stratification characteristics of both basins. When the outflow is associated with PV gradients of both signs, it may be unstable by the Charney–Stern criterion. This has been invoked, for instance, in [Spall and Price \(1998\)](#) to explain the generation of cyclones near Denmark Strait. However, when the intrusion of fluid has only a single sign for both its PV and its gradient, then it is linearly stable by the Charney–Stern criterion. This is thought to be the case for the Mediterranean current (e.g., [Marshall 1988](#); [Spall and Price 1998](#)), which is probably why several nonlinear eddy-generation mechanisms have been proposed that are not based on linear instability.

[Chérubin et al. \(1996\)](#) examines the influence of a canyon on the generation of vortices and shows that this topography can generate large-amplitude meanders that roll up into vortices. [Nof \(1991\)](#) studies eddy generation that ensues from a geostrophically unbalanced pulse in the current, caused by internal waves or atmospheric forcing. [Pichevin and Nof \(1996\)](#) study the influence of a cape on the generation of vortices in a reduced gravity model: analysis of the momentum budget shows that when a coastal current has a strong veering, it cannot be stationary so that anticyclonic vortices have to be generated to close the momentum budget. Because of the planetary beta effect (i.e., spatial variation of the Coriolis frequency), these anticyclones detach from the coast when they become large enough.

When gravity currents enter a basin and flow downhill, they undergo intense mixing with the surrounding waters ([Price and Baringer 1994](#)). For instance, the Mediterranean outflow current mixes with the Atlantic water ([Baringer 1993](#); [Rhein and Hinrichsen 1993](#); [Johnson et al. 1994](#); [Baringer and Price 1997a,b](#)) so that its potential density decreases from $\sigma_\theta \approx 29$ kg m^{-3} near the Strait of Gibraltar to $\sigma_\theta \approx 27.5$ kg m^{-3} in the Gulf of Cadiz. Since PV is not conserved when mixing occurs, one may wonder if intense mixing can sufficiently transform the PV distribution of an initially stable current into an unstable one capable of generating detached vortices.

This question is the subject of this paper. In [section 2](#) we recall some properties of PV and discuss its integral constraints as expressed in the Charney–Stern and Haynes–McIntyre relations. We show how these relations can be combined to explain how diapycnal and isopycnal mixing can yield unstable currents. We then use computational solutions to demonstrate this behavior in [section 3](#). In [section 4](#) we further demonstrate it with results from rotating-tank experiments on gravity currents. We conclude in [section 5](#) by summarizing our results and discussing their implications both in nature and in oceanic general circulation models (GCMs).

2. Potential vorticity constraints

Since the early work of [Rossby \(1939\)](#) and Ertel (1942), PV has been recognized as a useful quantity for interpreting the dynamics of the atmosphere and the ocean (e.g., [McWilliams and Gent 1980](#); [Hoskins et al. 1985](#); [McIntyre and Norton 1990](#)). Potential vorticity is a scalar quantity that combines the vorticity and potential density. Under the assumptions of hydrostatic and geostrophic or gradient-wind balance, the global distribution of PV uniquely determines the simultaneous velocity field, given appropriate boundary conditions. If the evolution is adiabatic, potential density and PV are conserved along trajectories, and anomalies in the PV field are constrained to remain on surfaces of constant potential density that are monotonically ordered in a stably stratified fluid.

For a stably stratified fluid in hydrostatic balance, we can transform the dynamical equations into isopycnal coordinates, where the effective vertical coordinate is the potential density. Here PV is defined by

$$\text{PV}_{\text{Ertel}} = \frac{\zeta + f}{h}, \quad (1)$$

where $\zeta = \text{rot}(\mathbf{U}) = \partial_x \mathbf{v} - \partial_y u$ is the curl of the velocity field $\mathbf{U} = (u, \mathbf{v})$ in the direction perpendicular to an isopycnal surface, f is the Coriolis frequency (which we assume to be spatially constant in this paper), and $h = \partial_\rho z$ is the differential thickness of an isopycnal layer ([Cushman-Roisin 1994](#)).

As pointed out by Ertel (1942), PV can have alternative definitions since multiplying [\(1\)](#) by any function of the potential density yields a quantity with the same properties of Lagrangian conservation and the possibility of diagnostically evaluating the 3D velocity field. Using $H = h_{\text{rest}}$ the stratification of the fluid at rest (i.e., the state achieved by adiabatically rearranging the density field until its iso-surfaces are flat), we define the PV anomaly (PVA) by

$$\begin{aligned}\Delta Q &= H \times (\text{PV}_{\text{Ertel}} - \text{PV}_{\text{Ertel}}^{\text{ref}}) = H \times \left(\frac{\zeta + f}{h} - \frac{f}{H} \right) \\ &= \frac{H}{h} \left(\zeta - f \frac{\Delta h}{H} \right),\end{aligned}\quad (2)$$

where $\Delta h = h - H$. In the last relation we recognize the vorticity term ζ and the stretching term $f\Delta h/H$, which are the familiar components of PV in the quasigeostrophic approximation. Indeed, when the quasigeostrophic assumptions are valid, [Eq. \(2\)](#) is equivalent to the quasigeostrophic PV formula; see [section 2a](#).

For simplicity in this paper, we will consider a model ocean with a countable sequence of layers of constant density stacked on top of each other in a stable configuration (see [Fig. 1](#)). In this case, in the previous formulas h and H can be interpreted as the thicknesses of the discrete layers. All theoretical results derived in the rest of this section can be generalized to continuously stratified flows.

a. Charney–Stern necessary condition for instability

When the Rossby number is small and the Burger number at least order one (which corresponds to a situation for which the layer thickness variation Δh is small when compared to H), the quasigeostrophic model can be derived ([Pedlosky 1987](#)). This approximate model advectively conserves the quasigeostrophic PV,

$$\text{PV}_{\text{QG}} = \zeta - f \frac{\Delta h}{H}, \quad (3)$$

along horizontal trajectories, and each of the advecting velocity, the relative vorticity ζ , and the stretching term $-f\Delta h/H$ is a diagnostic linear functional of the streamfunction (or pressure field).

For this model Charney and Stern (1962, hereafter C–S) shows that a necessary condition for a mixed barotropic–baroclinic instability to occur for a steady zonal flow is that the meridional gradient of $\overline{\text{PV}}_{\text{QG}}(y, z)$ change sign somewhere in the current. Using the approximate equivalence of PV_{QG} and the PVA in [\(2\)](#), this criterion can be written as

$$\text{INSTABILITY} \Rightarrow \partial_y(\overline{\Delta Q}) > < 0,$$

where $A > < 0$ indicates that A assumes both signs in different regions. The C–S result is only for the quasigeostrophic model, but it has recently been extended to semigeostrophic flows (see [Kushner 1995](#)). Also, the barotropic/baroclinic stability conditions derived by [Ripa \(1991\)](#) for a multilayer, shallow-water model through analysis of the energy of the perturbations indicate that the C–S criterion is valid more generally. The C–S criterion is also valid for mean coastal currents next to a parallel boundary with no normal flow through it.

We can distinguish two different configurations that satisfy the C–S criterion for instability.

1. The gradient of the PVA changes sign along an isopycnal surface (or within a vertical layer). This situation is depicted in [Fig. 2a](#).
2. The gradient changes sign in different layers. This situation is depicted in [Fig. 2b](#).

In this paper, we will focus on the second case, where the PVA is monotonic in each layer but has different sign in different layers. For such a configuration, as shown for instance in [Shen and Evans \(1994\)](#), a common outcome of the instability is the detachment of a baroclinic vortex pair, sometimes called a heton ([Hogg and Stommel 1985](#)), which has two PVA centers of opposite sign located in different layers. Three stages of the instability are depicted in [Fig. 3](#). An initial meander of the positive PVA front is associated with a cyclonic circulation over the whole water column and thus generates a perturbation on the negative PVA front below (dashed line in [Fig. 3a](#)). The latter is associated with an anticyclonic circulation over the whole water column (dashed line in [Fig. 3b](#)), and both meanders tend to reinforce each other. When they are large enough, the meanders detach from the current and form a baroclinic dipole ([Fig. 3c](#)). The emergence of such a structure is accompanied by a transfer of mean potential energy to the eddy kinetic energy; hence the instability depicted in [Fig. 3](#) is primarily a baroclinic instability.

Now consider a coastal current with a PVA localized near the boundary and $\Delta Q \rightarrow 0$ away from the boundary. This corresponds to the downstream situation of an intruding water mass flowing into a basin along its coast. For the current as a whole, integrating the C–S criterion yields

$$\text{INSTABILITY} \Rightarrow \overline{\Delta Q} > < 0.$$

Thus, the necessary condition for baroclinic instability of a coastal current whose PVA is localized near the boundary is that ΔQ changes sign in different layers.

b. Haynes–McIntyre impermeability constraint

When mixing does occur, it is not easy to predict the change of PV for a fluid parcel, even if the trajectory is known, since the outcome is a nonlinear combination of the mixing of momentum and density. Nevertheless, [Haynes and McIntyre \(1987, 1990\)](#), hereafter H–M) derive an integral constraint for the evolution of PV. Here we rederive it for a multilayer, shallow-water model. In this context ([Bleck and Boudra 1986](#); [Bleck and Smith 1990](#); [Bleck et al. 1992](#); [Hu 1996](#)), the momentum and thickness equations for each layer are

$$\begin{aligned} \partial_t U + (\mathbf{U} \cdot \nabla)U - fV &= -\partial_x M + F_x \\ \partial_t V + (\mathbf{U} \cdot \nabla)V - fU &= -\partial_y M + F_y \\ \partial_t h + \text{div}(h\mathbf{U}) &= S. \end{aligned} \quad (4)$$

Here $\mathbf{U} = (U, V)$ is the horizontal velocity field, h is the layer thickness, and M is the Montgomery potential (pressure along an isopycnal surface), which can be expressed in each layer k as a linear combination of all the layer thickness anomalies [$i = (1, \dots, N)$, where N is the number of layers],

$$M_k = \sum_{i=1}^{i=k-1} \frac{\rho_i}{\rho_k} g \Delta h_i + \sum_{i=k}^{i=N} g \Delta h_i. \quad (5)$$

Here $\mathbf{F} = (F_x, F_y)$ and S are nonconservative terms representing mixing, which we formulate as Fickian diffusion (for instance, the source term S in the continuity equation is associated with a density diffusion $\dot{\rho} = \partial_z K_\rho \partial_z \rho$). In isopycnal coordinates they are expressed as follows (see [Hu 1996](#); [Hallberg 1999](#)):

$$\begin{aligned} F_x &= \partial_x(\nu \partial_x U) + \partial_y(\nu \partial_y U) + \frac{d\rho}{h} \partial_\rho \left(\frac{K_u d\rho}{h} \partial_\rho U \right) \\ F_y &= \partial_x(\nu \partial_x V) + \partial_y(\nu \partial_y V) + \frac{d\rho}{h} \partial_\rho \left(\frac{K_u d\rho}{h} \partial_\rho V \right) \\ S &= -\partial_\rho^2 \left(\frac{K_\rho d\rho^2}{h} \right). \end{aligned} \quad (6)$$

The horizontal diffusion coefficient ν is defined by $\nu = \max(\nu_0, \nu_{\text{Smag}})$, where ν_0 is a background constant, and, following Smagorinsky (1963), ν_{Smag} is the product of the deformation rate (i.e., $|\nabla \mathbf{U}|$), the square of the horizontal grid size, and a coefficient C_s . The values of C_s or ν_0 as well as forms for the diapycnal coefficients, K_u and K_ρ , are specified in [section 3](#). The coefficient $d\rho$ represents the density jump between layers. Taking the curl of the momentum equation yields

$$\partial_t(hPV_{\text{Ertel}}) = -\text{div}(hPV_{\text{Ertel}}\mathbf{U}) + \text{rot}\mathbf{F}. \quad (7)$$

Integrating over a domain Ω with periodic boundary conditions or boundaries with no normal flow through it (e.g., vertical walls) gives

$$\frac{d}{dt} \iint_{\Omega} \text{PV}_{\text{Ertel}} h \, dx \, dy = \int_{\partial\Omega_{\text{wall}}} \mathbf{F} \cdot d\mathbf{l}, \quad (8)$$

where $\int_{\partial\Omega_{\text{wall}}} \mathbf{F} \cdot d\mathbf{l}$ represents the circulation of \mathbf{F} along boundaries representing vertical walls only. This last condition shows that the bulk integral of PV within a density layer is not changed by either diapycnal or isopycnal mixing as long as it occurs away from the boundaries, which is the H–M constraint.

Using the definition (2) for the PVA and as $d\Omega = h \, dx \, dy$ is a volume element, we can rewrite the previous H–M constraint (8) in terms of the PVA as follows:¹

$$\frac{d}{dt} \iiint_{\Omega} \text{PV}_{\text{Ertel}} \, d\Omega = \frac{d}{dt} \iiint_{\Omega} \left(\frac{f}{H} + \frac{\Delta Q}{H} \right) d\Omega \quad (9)$$

$$= \int_{\partial\Omega_{\text{wall}}} \mathbf{F} \cdot d\mathbf{l}, \quad (10)$$

which yields

$$\frac{d}{dt} \iiint_{\Omega} \Delta Q \, d\Omega = -f \frac{d\Omega}{dt} + H \int_{\partial\Omega_{\text{wall}}} \mathbf{F} \cdot d\mathbf{l}, \quad (11)$$

where $d\Omega/dt$ represents the volume variation of the layer. Thus, the bulk integral of the PVA can only be changed by a depletion or gain of the volume inside a layer or by viscous effects along boundaries.

c. Effects of diapycnal mixing

Although the H–M constraint does not tell us explicitly about the local PVA evolution of a parcel, we can use it as a rough guideline to guess what the PVA distribution looks like after mixing. Neglecting the effects of the viscous boundary layer [e.g., the last term in (11)], if, for instance, during a diapycnal mixing event the volume of a layer increases, then the integral of PVA decreases and a negative PVA is generated somewhere within the layer. If, on the contrary, volume is lost in the layer, a positive PVA is generated.

This argument has been successfully used in the atmosphere to predict cyclogenesis (through the creation of a positive PVA) due to breaking gravity waves in the lee of steep mountain chains (Lamarque 1993; Lamarque and Hess 1994; Keyser and Rotunno 1990). In the open ocean, Legg and Marshall (1993) and Legg et al. (1998) show that the PV flux associated with winter cooling at the surface followed by internal mixing by spatially inhomogeneous deep convection creates a negative PVA in the underlying water column, while the adjacent front associated with the surface outcropping of density layers can be represented by a surface sheet of positive PVA. In this situation baroclinic instabilities develop, and the PVA is subsequently spread laterally by hetonlike vortices.

When mixing occurs in the interior of the fluid without any PV fluxes from the boundaries, then (11) implies that PVA creation depends upon the mass change within a density layer. Consider a fluid with uniform PV initially (for instance a fluid at rest), then $\Delta Q = 0$ everywhere (Fig. 4a). If interior diapycnal mixing occurs, water will be transferred between layers subject to conservation of total water volume. The H–M constraint says that negative PVAs must be created in layers where mass increases and positive ones created in layers where it decreases. This gives rise to a current associated with opposite sign PV anomalies in different layers (Fig. 4b). The C–S criterion says that this current is potentially baroclinically unstable. Thus, diapycnal mixing in the interior of the ocean can lead to baroclinically unstable currents.

The rate at which PVA is created through diapycnal mixing can be roughly estimated using (11) and (6) as

$$O(\Delta Q)_{\text{diap}} \approx f \frac{K_{\rho}}{h^2} \delta t. \quad (12)$$

This yields a time period of a few days for the development of a PVA $\Delta Q \approx 0.1f$ (with $K_{\rho} = 250 \text{ cm}^2 \text{ s}^{-1}$ and $h = 250$

m).

d. Effects of isopycnal mixing

As far as isopycnal mixing is concerned, we distinguish two different situations depending on whether we consider its effect in the interior of the ocean or near boundaries where a viscous layer is present.

In the ocean interior, the H–M constraint (11) shows that mixing does not alter the average PVA of a layer. However, isopycnal mixing can modify the local PVA and either smooth the initial PV field, which should not change the stability property of a current, or create opposite sign PVAs (but not change the bulk integral of PVA), which could lead to the destabilization of currents. Growth rates of an initially unstable current have been shown to be sensitive to momentum dissipation (Holopainen 1961; Rivière 1995; Rivière and Klein 1997), but, to our knowledge, an example of the destabilization of an interior current by isopycnal mixing has not been found.

Near a boundary the effects of a viscous layer have to be taken into account, and Eq. (11) shows that it generally alters the mean PVA of the layer. It is not clear, though, if this alteration yields unstable PVA profiles that satisfy the C–S necessary condition. Indeed, the sign of the created PVA depends on second-order derivatives of the velocity field near the coast. In addition, in numerical models, it may be sensitive to the boundary conditions used (e.g., free slip or no slip). As above, one can calculate the timescale required for the development of a significant PVA through isopycnal mixing. A rough estimate is

$$O(\Delta Q)_{\text{isop}} = \frac{\Delta U \nu}{\Delta L^3} \delta t, \quad (13)$$

where ΔU is the scale of velocity differences and ΔL represents the width of the region affected by mixing and depends on both the viscous layer thickness and the velocity field variation length scale. This yields a time period of a few days for the development of a PVA with $\Delta Q \simeq 0.1f$ (using $\nu = 10 \text{ m}^2 \text{ s}^{-1}$, $\Delta L = 5 \text{ km}$ and $\Delta U = 0.2 \text{ m s}^{-1}$).

This suggests that isopycnal mixing could be as efficient as diapycnal mixing in creating PVAs. However, these estimates are sensitive to the choices for the diapycnal or isopycnal mixing coefficients, stratification strength, and velocity magnitude. Different choices of isopycnal mixing forms (biharmonic diffusion of momentum for instance) or even boundary conditions may also yield different results. Nevertheless, the important conclusion here is that isopycnal or diapycnal mixing could drastically modify the PV distribution in an oceanic current in only a few days.

3. Computational experiments

The qualitative prediction of instability above is not a rigorous one. The C–S criterion is only a necessary condition for instability, and the H–M constraint does not predict in detail the local PVA evolution. The situation depicted in Figs. 4a and 4b is thus only a thought experiment. Computational or laboratory experiments, or field measurements, are needed to assess the likelihood of such an evolution in the ocean, and below we present samples of all three.

To illustrate that diapycnal or isopycnal mixing can lead to baroclinically unstable currents, we first perform some computational experiments. We do so with an ocean model in isopycnal coordinates, where it is easier to control the isopycnal PVA evolution and the diapycnal mass fluxes, particularly when, as here, the number of vertical degrees of freedom (i.e., density layers) is not large. The model is the Miami Isopycnal Coordinate Ocean Model (MICOM: see Bleck and Boudra 1986; Bleck and Smith 1990; Bleck et al. 1992; Hu 1996), which solves Eqs. (4)–(6).

a. Currents initiated by diapycnal mixing

The first experiment realizes the thought experiment sketched in Fig. 4. We consider a five-layer configuration with equal density steps $\Delta\rho = 0.2\%$ between layers and layer thickness $H = 400 \text{ m}$. The fluid is initially at rest, with $\mathbf{U} = 0$ and $h = H$. The horizontal grid size is 2 km, and the domain is a zonally periodic channel of size 200 km \times 200 km, with free-slip boundary conditions at the northern and southern walls. The Coriolis frequency is $f = 7.0 \times 10^{-5} \text{ s}^{-1}$. The horizontal viscosity is constant (i.e., $C_s = 0$ here) with a small value $\nu_0 = 0.1 \text{ m}^2 \text{ s}^{-1}$ chosen for computational smoothness. Here the PV fluxes from viscous boundary layers are negligible, and the PVA is only transformed because of diapycnal mixing. (Alternative experiments with $C_s = 0.005$, rather than the usual value of 0.2 for 3D turbulence, lead to the same results.)

At $t = 0$, the resting fluid undergoes vigorous diapycnal mixing near the southern boundary. To accomplish this we set $K_u = K = 200 \times 10^{-4} \text{ m}^2 \text{ s}^{-1}$ within 10 km of the coast and at the upper and lower interfaces of the third layer, while keeping

$K_u = K_\rho = 0$ elsewhere. Estimated values for K_u and K_ρ are usually smaller in the open ocean than those above, but this level of mixing has been observed in some regions ([Peters and Gregg 1988](#); [Baringer and Price 1997b](#); [Ferron et al. 1998](#)) and has been implemented in mixing parameterizations (e.g., [Blanke and Delecluse 1993](#); [Large et al. 1994](#)). In any event, smaller values of K_u and K_{rho} would only lengthen the time period over which the current spins up and its instability develops.

[Figure 5](#) shows the evolution of the PVA in the third and fourth layers (counting down from the upper surface). Because the mixing coefficient is largest in the middle of the water column, the third layer gains mass while the second and fourth layers lose mass. A negative PVA is thus created in the third layer, and positive PVAs in the second and fourth layers, as sketched in [Fig. 4](#). During the mixing, geostrophic adjustment takes place continually, and a baroclinic zonal current is generated near the southern boundary. [Figure 5](#) shows that, after about 20 days, the PVA of the current has become fairly strong (its minimum value in the third layer is $-0.2f$). At this stage we added a small nonzonal perturbation. Since the PVA distribution of this current satisfies the C–S criterion, we might expect baroclinic instability to develop. Instability indeed rapidly develops and meanders grow. This leads to the formation of baroclinic dipoles or hetons that detach from the coast and move out toward the open ocean. [Figure 6](#) shows the velocity field in these two layers at $t = 70$ days. The negative PVAs are associated with anticyclonic vortices, and the positive PVAs with cyclones, as expected from geostrophic balance.

In this experiment we did not consider the cause of the localized mixing. One possibility, though, is mixing associated with gravity waves breaking above a continental shelf or bottom topography. Such a process might explain the formation of swoddies (slope water eddies) in the Gulf of Biscay ([Pingree and Le Cann 1992a,b](#); [Pingree 1994](#)).

b. Currents modified by mixing

In the preceding experiment, the fluid is initially at rest, and the mixing coefficients are specified as functions of space. To show how diapycnal or isopycnal mixing can modify the stability of an existing current, we next consider a zonal bottom current associated with an initially stable PVA distribution and in geostrophic balance. We consider a seven-layer configuration with density jumps between the layers, $\Delta\rho = 0.2\%$, and resting fluid layer thicknesses, $(H_1, H_2, H_3, H_4, H_5, H_6, H_7) = (500 \text{ m}, 100 \text{ m}, 100 \text{ m}, 100 \text{ m}, 100 \text{ m}, 100 \text{ m}, 500 \text{ m})$. The initial PVA distribution has $\Delta Q = 0$ in layers 1–6 and has a strong perturbation in the bottom layer:

$$\Delta Q_7(y) = -0.7fe^{-(y/L)^2}, \quad (14)$$

where y is the distance from the southern coast and $L = 30 \text{ km}$. The Coriolis frequency is $f = 7 \times 10^{-5} \text{ s}^{-1}$.

The calculation of the initial velocity field and layer thicknesses corresponding to the PVA profile given above is done by iteration between (2) and geostrophic balance, subject to the constraints that $U \rightarrow 0$ away from the southern boundary and that $U(z)$ is specified at the southern coast (see the appendix).

We solve [Eqs. \(4\)–\(6\)](#) numerically, first in a 2D configuration with no zonal variations ($\partial_x = 0$ for all quantities) to evaluate the PV changes associated with both diapycnal and isopycnal mixing, and then in a 3D configuration to investigate ensuing instabilities. The meridional extent of the basin is $L_y = 140 \text{ km}$ and the horizontal grid size is 2 km . In such a 2D configuration, alongstream, small-scale numerical noise cannot develop, and weaker background isopycnal diffusivities can be used while still retaining solution smoothness.

Isopycnal and diapycnal mixing effects are studied separately. To study the effect of isopycnal mixing of momentum on the destabilization of the current, different values of ν_0 are chosen; we set $\nu_0 = 1\text{--}20 \text{ m}^2 \text{ s}^{-1}$ in various calculations, which is less than the typical range used in eddy-resolving GCM calculations. The effect of a biharmonic diffusion, with coefficient $\nu_{BH} \cong 10^8 \text{ m}^4 \text{ s}^{-1}$, is also investigated. To study the influence of diapycnal mixing, we follow [Pacanowski and Philander \(1981\)](#) and specify the diapycnal diffusivities, K_u and K_ρ , as functions of the gradient Richardson number, $\text{Ri} = N^2/|\partial_z U|^2$ (where N is the Brunt–Väisälä frequency):

$$K_u = \frac{K_o}{1 + \text{Ri}/\text{Ri}_o}, \quad K_\rho = \frac{K_u}{1 + \text{Ri}/\text{Ri}_o}, \quad (15)$$

where either $K_o = 0$, in cases where diapycnal mixing is neglected, or $K_o = 500 \times 10^{-4} \text{ m}^2 \text{ s}^{-1}$. Notice that the value for

K_u monotonically decreases with Ri and exceeds that of K_ρ for all Ri. In the following simulation, $Ri_o = 1$, which corresponds to the minimum Richardson number of the flow defined by (14) and the boundary conditions discussed in the appendix. The particular functional form chosen here extends the mixing well beyond the critical value for Kelvin–Helmholtz instability, for which mixing is known to occur for $Ri \leq Ri_{cr} = 0.25$ (see Miles 1961; Howard 1961). In fact, geostrophic currents with weak Richardson numbers are necessarily associated with strong velocities, and rather high horizontal diffusion coefficients are then necessary to maintain the solution smoothness. To be able to get solutions in which the PVA is mainly modified by diapycnal mixing, we choose to consider currents with higher Ri values and to extend mixing far beyond the theoretical value of 0.25. Even though this choice is quantitatively questionable, and thus impedes a precise linkage to oceanic situations, the previous parameterization is qualitatively as observed in the ocean for the mixing associated with shear instability, where regions of smaller Ri are likely to be more sensitive to shear instability and subsequent mixing if, for instance, gravity waves are present in addition to the geostrophic currents. It can thus serve our purpose here of illustrating possible consequences of mixing.

Figure 7 shows the vertical PVA distribution at time $t = 10$ days in 2D integrations for different choices of the mixing coefficients K_o and (v_o, C_s) listed in Table 1. Figure 7a represents a case with no mixing (isopycnal or diapycnal), for which the PVA profile corresponds to the initial PVA distribution. It is null in all layers except the last, is associated with a one-sign gradient, and is therefore stable by the C–S criterion. In Fig. 7b, a weak isopycnal mixing is included. The PVA distribution is not significantly modified for the period of time considered here (10 days). In Fig. 7c, diapycnal mixing is added. Obviously diapycnal mixing leads to the creation of opposite-sign PVAs of significant strength (the maximum positive PVA reaches about $0.1f$ at the surface and 500 m, $0.2f$ at 1000 m) and satisfying the C–S necessary condition for instability. The influence of strong isopycnal mixing is shown in Fig. 7d. Stronger modifications occur in comparison with Fig. 7b, and positive PVA now appears (the maximum reaches $0.15f$), rendering the distribution potentially unstable. Finally, a solution with biharmonic diffusion of momentum is shown in Fig. 7e, with a moderate diffusivity coefficient of $v_{BH} = 10^8 \text{ m}^4 \text{ s}^{-1}$. The viscous boundary layer has here drastically modified the PVA distribution and a very strong positive PVA has developed, with the maximum value reaching $0.7f$. Notice that this positive PVA is located in a narrow region near the coast where the viscous boundary layer develops. Also notice that the negative PVA in the bottom layer has been strongly modified too in that case.

We next continue the same integrations in a zonally periodic, 3D channel with length $L_x = 200$ km, to test for the stability of the current and development of meanders. A very small initial, nonzonal perturbation is added to the zonal current. In this 3D configuration, the isopycnal viscosity coefficients (v_o, C_s) cannot be zero, and minimum values (below which numerical noise develops and the computation must be stopped) must be specified, which sometimes makes it difficult to distinguish between the influence of diapycnal and isopycnal mixing. We choose here the minimum values of $(v_o, C_s)_{\min} = (1 \text{ m}^2 \text{ s}^{-1}, 0.005)$. We have shown above that such small values have only weak effects on the PVA field (see Fig. 7b). However, if the current changes when it becomes unstable and meanders grow (for instance when diapycnal mixing is taken into account), higher minimum values are necessary. In that case, we choose to increase C_s , and values as high as $C_s = 1$ are sometimes necessary to keep small-scale noise from growing. However, this only affects the late-stage evolution of the PVA.

Without diapycnal mixing and with a small isopycnal diffusion ($v = 1 \text{ m}^2 \text{ s}^{-1}$), the current remains stable for more than 200 days. When diapycnal mixing is added, the evolution is quite different, and Fig. 8 shows that the current now becomes unstable. As shown above, a positive PVA develops quite rapidly in the upper layers, allowing the current to become potentially unstable according to the C–S criterion. The formation of the positive PVA is quite rapid, requiring only a few days, but the subsequent growth of meanders and generation of vortices, on the other hand, are slower processes, partly because the initial perturbation is small; the growth rate σ has been roughly evaluated from the solution and corresponds to a timescale of $T_{\text{growth}} = 1/\sigma \simeq 10$ days, and meanders are clearly visible after 100 days. At this stage, small-scale noise develops near the southern boundary, and we have to increase C_s up to 1 to erase this numerical noise. However, an experiment with $C_s = 0.05$ has also been made, which although noisy remains computationally stable. The results differ in detail between strong and weak C_s , but in both cases baroclinic dipoles eventually emerge and detach from the boundary current.

As mentioned above, in experiments without diapycnal mixing and with a weak momentum diffusion coefficient ($v_o = 1 \text{ m}^2 \text{ s}^{-1}$), the current remains stable. Increasing this coefficient strengthens the boundary flux of PV and transforms the current profile into a potentially unstable configuration (see Figs. 7d,e). Three-dimensional solutions for experiments d and e in Table 1 indeed also exhibit an unstable behavior after about 100 days and 50 days, respectively. The destabilizing influence of the lateral mixing of momentum on boundary currents is also studied in Valdivieso da Costa (1999). In her numerical solutions for a current intruding into a quiescent fluid, she observed that biharmonic diffusion of momentum leads

to the generation of positive PVA in the layer above the intrusion and can lead to the detachment of baroclinic dipoles.

The effect of a viscous boundary layer on the generation of eddies in a barotropic model is investigated in [d'Asaro \(1988\)](#) and [Klinger \(1993\)](#). They argue that mixing near a boundary is a source of preferentially negative PVA generation, which can roll up into anticyclonic eddies at capes. In our experiments, PVA develops in viscous boundary layers, but its sign strongly depends on the current profile near the wall and is proportional to v . The PV flux also depends on the boundary condition imposed, and it is worth mentioning that both free-slip and no-slip conditions generally lead to nonzero fluxes. Furthermore, in this set of experiments, PVA generation is very sensitive to the mathematical form chosen to parameterize mixing: biharmonic diffusion leads to the development of much higher PVAs than harmonic diffusion. Zero fluxes could theoretically be obtained if the boundary condition yields $\mathbf{F} \cdot \mathbf{dl} = 0$ along the boundary, but this is not easily justified physically and it is difficult to achieve in practice because of the spatial discretization, the use of a staggered grid, or the presence of inclined boundaries in GCMs. However, we have here shown that a cape is not necessary for the formation of vortices, as the PVA generation associated with the viscous boundary layer can yield unstable situations in a stratified fluid. Incidentally, it is worth mentioning that, for homogeneous flows, rotating-tank experiments seem to indicate that, even though a cape seems to be a preferential site for the formation of eddies, their detachment is only possible if the current upstream of the corner is barotropically unstable to the formation of dipoles ([Klinger 1993](#); [Stern and Whitehead 1990](#)).

To conclude, we note that, in the ocean, the physical nature of PVA generation by isopycnal mixing is uncertain but nonetheless possible. Indeed, isopycnal mixing represents the effect of subgrid-scale, anisotropic currents along isopycnal surfaces, and to our knowledge there is no clear evidence showing such processes should or should not be associated with large-scale PV generation. We have demonstrated that this issue can have important consequences for the stability of currents.

4. Laboratory experiments

Diapycnal mixing is usually intense in gravity currents. This suggests that these currents will develop a PVA distribution that satisfies the C–S criterion and thus become potentially baroclinically unstable. Extending the computations above to a simulation of gravity currents is quite challenging because of nonhydrostatic accelerations and complex mixing effects and also because the existing numerical schemes do not accurately conserve PV in a configuration when isopycnal surfaces intersect the bottom topography. Consequently, we choose to switch our methodology to laboratory experiments to investigate the evolution of rotating gravity currents.

a. Experimental setup

The experimental setup is sketched in [Fig. 9](#). It is the same as in [Mauritzen et al. \(2001\)](#), a study of the detrainment of Mediterranean Water to low density levels. A rotating tank with horizontal dimensions $80 \text{ cm} \times 80 \text{ cm}$ contains a continuously stratified fluid initially at rest. An approximately constant Brunt–Väisälä frequency, $N \simeq 0.5 \text{ s}^{-1}$, is constructed using the two-reservoir method ([Fortuin 1960](#)). The rotation period is $T = 20 \text{ s}$, giving a Coriolis frequency of $f = 0.63 \text{ s}^{-1}$. The total fluid depth is $H \simeq 20 \text{ cm}$. The first internal radius of deformation is $R_d = HN/\pi f \simeq 5 \text{ cm}$. Since this scale is similar to the width of a geostrophically adjusted boundary current, we believe that the tank is wide enough for distant boundary influences to be small.

A colored plume of dense water is gently poured from a reservoir at a position near the corner on top of a sloping bottom on one side of the tank (see [Fig. 9](#)). Its density anomaly, compared to the surface fluid in the tank, is $\Delta\rho \simeq 5\%$, which is about the same as the maximum density anomaly at the bottom of the tank. The bottom slope is fairly steep, with $s = dx/dz \simeq 0.4$. The dense fluid accelerates as a plume that sinks down the slope. When the vertical shear at the top of the plume current is strong enough, Kelvin–Helmholtz instability occurs, and the plume entrains and mixes with the surrounding water. Eventually the plume arrives at an equilibrium depth, where its intermediate density value is neutrally buoyant compared to the surrounding fluid, and it then turns to form a coastal current as it leaves the slope following the sidewall boundary. Even though the hydrostatic approximation is not strictly satisfied in this experiment, rotation and stratification inhibit vertical motions, and the boundary current rapidly adjusts toward geostrophic balance, during and after the strong mixing phase. The experiment is photographed and filmed from both the top of the tank and the side parallel to the boundary current.

b. Experimental results

[Figure 10](#) is a photograph taken from a side of the tank. The red color corresponds to the intermediate-depth current. Since the red color has become well mixed within the current by this stage, it is difficult to clearly distinguish its structure here. So additional dye grains are dropped through the boundary current to give an indication of its vertical profile. The strongest velocity occurs at middepth.

[Figures 11a–c](#) are successive photographs taken from the top of the tank. The coastal intermediate current is visible

along the left side of the tank. We see a downstream and temporal evolution of an instability event and the subsequent generation of a baroclinic vortex dipole. The dipole structure is indicated by the mushroom shape erupting from the boundary region (see [Mied et al. 1991](#)). The anticyclonic vortex center is a lens of red fluid, and the cyclonic vortex center wraps filaments of red fluid around itself. Using additional drops of dye grains (not shown), we find that the anticyclone has its maximum swirl velocity maximum at approximately the same depth as the coastal current, while the cyclone maximum velocity occurs above the core of the boundary current but slightly below the surface. This demonstrates the baroclinic (i.e., hetonic) structure of the dipole vortex. If the experiment is allowed to evolve over sufficient time, the intermediate flow sheds these dipolar eddies around the entire tank.

The formation of such a flow structure is typical of baroclinic instability. It requires the presence of both positive and negative PVAs. The negative PVA is the anticyclonic part of the dipole. It arises in the injected water mass that forms the core of the boundary current and, as argued above from the H–M constraint (11), it develops because the core density layers gain mass and grow in thickness. The upper-level cyclone has a positive PVA, associated with the depletion of mass and reduction of thickness in the density layers mainly above the core of the boundary current. This interpretation neglects possible PVA effects from the viscous boundary layer, which we believe is of only secondary importance here, due to the smallness of the molecular viscosity.


5. Discussion

In this paper we show that mixing can alter a current and make it unstable, generating baroclinic dipoles or hetons. Potential vorticity (PV) is not conserved on parcels when mixing occurs. Even though it does not prescribe the PV change in detail, the integral constraint in [Haynes and McIntyre \(1987, 1990\)](#) suggests the likely shapes of PV anomalies (PVAs) that arise from diapycnal mixing: positive PVA is created where a density layer loses mass and negative PVA is created where a layer gains mass. These transformations of the PVA distribution allow an initially stable current to satisfy the instability criterion of [Charney and Stern \(1962\)](#), in a manner conducive to baroclinic instability. In turn, baroclinic instability can evolve into heton vortices that detach from the current and move into the fluid interior. Strong diapycnal mixing is especially likely near boundaries. It can be associated with gravity waves breaking over a steep continental shelf, with Kelvin–Helmholtz instability due to strong vertical shear, or with downslope gravity currents.

This possibility is illustrated with highly idealized computational and laboratory experiments. We make no claim, yet, that these behaviors are generic since the outcome may be sensitively dependent upon the flow characteristics and mixing patterns (parameterized here in the computational experiments as a function of the Richardson number) that we have not explored widely. Nor do we feel confident that the range of mixing intensity that occurs in the ocean near outflows and shallow boundaries is yet well known. Nevertheless, we believe this mode of PVA generation and subsequent eddy formation is likely to occur in the ocean at least sometimes. As suggested by an anonymous referee, it would be useful to calculate PV maps along isopycnal surfaces from transects at various distances from the Strait of Gibraltar. Even though large errors can be expected for the calculation of PV on isopycnal surfaces from measurements at sea, it could prove useful in explaining the influence of mixing on PV evolution. Cross sections of PV have been calculated by [Chérubin et al. \(2000\)](#) near the Portimao Canyon. They show that the C–S instability criterion is met for the Mediterranean outflow in this area far downstream of Gibraltar.

Isopycnal mixing and diffusion of momentum is usually associated with PV fluxes from boundaries, that can create new PVAs. Again, this transformation of the PV distribution is shown to be able to destabilize the current if the diffusion coefficient is large enough. The physical relevance of this phenomenon is, however, uncertain and has to be addressed. Our numerical experiments have also revealed drastic differences in the PVA generation, depending on whether harmonic or biharmonic operators are used (different boundary conditions can also lead to substantial changes). Thus, in numerical models, diffusion terms could generate PVA that is quantitatively questionable, especially near boundaries, and thus result in discrepancies with respect to the real ocean.

It is finally worth mentioning that this work has some implications insofar as GCMs are concerned. We have indeed shown here that the dynamics of a boundary current in a numerical model is very sensitive to both diapycnal and isopycnal mixing. In particular, PV fluxes through boundaries can drastically change depending on the form chosen to parameterize isopycnal mixing, the diffusion coefficient values, and boundary conditions. Thus, different current regimes may be obtained with different choices of mixing parameterizations, insofar as the strength and the rate of formation of eddies are concerned.

We conclude by showing some field measurements that support the scenario above. The Sortie des Eaux Méditerranéennes dans l'Atlantique Nord Est (SEMANE) campaigns by the French Naval Oceanographic Service (SHOM) studied the Mediterranean current flowing along the Iberian continental slope. Particular attention was given to the formation of anticyclonic Mediterranean eddies (meddies), and a few surdrift floats were released in the main boundary current and followed daily by ARGOS satellites. Surdrift floats are deep drogued buoys, developed by SHOM and made of a small surface buoy linked to a large holey-sock drogue by a thin Kevlar cable ([Lampert 1998](#); [Chérubin et al. 1997](#); [Paillet et al. 1999](#)). In [Fig. 12](#) , two of these floats, respectively drogued at depths of 1000 and 1300 m, are apparently trapped in the same meddy generation event. The float at 1000 m loops anticyclonically in the core of the meddy, but the deeper float

subsequently begins to loop cyclonically and is clearly caught inside a companion cyclone. These features are consistent with the baroclinic instability of the Mediterranean boundary current and subsequent generation of a baroclinic dipole. The source of the positive PVA necessary for the instability and generation of the cyclone could have arisen from diapycnal mixing near the Strait of Gibraltar ([Baringer and Price 1997a](#)) or even downstream, in regions where the current is subject to strong mixing. Cyclonic companions for Meddies have been observed before; for instance, [Pingree and LeCann \(1993\)](#) show their signature in satellite advanced very high-resolution radiometer measurements.

Acknowledgments

We thank Rainer Bleck and Eric Chassignet for use of the MICOM code. The rotating-tank experiments were carried out in collaboration with Dr. Cecilie Mauritzen for a different study. We thank Alain Colin de Verdière, Lionel Scoarnec, Nicolas Perenne, Stephane Pous, and Jean-Michel Baey for their help with the rotating-tank experiments, and J. F. Lamarque and Sonya Legg for discussions. Finally, we thank Christophe Vrignaud who prepared [Fig. 12](#). This paper is a contribution to the SEMANE program conducted by SHOM and funded by the French Ministry of Defense (Grant PEA982401). Support for JCM was provided by the U.S. Office of Naval Research (Grant N00014-98-1-0165).

REFERENCES

- Baey J. M., 1997: Instabilités d'un courant d'eau intermédiaire. Thèse de doctorat de l'Université Joseph Fourier, Grenoble, France, 201 pp.
- Baringer M. O., 1993: Mixing and dynamics of the Mediterranean outflow. Ph.D. thesis, Massachusetts Institute of Technology/Woods Hole Oceanographic Institution Joint Program in Oceanography, WHOI-93-52, 244 pp. [Available from Woods Hole Oceanographic Institute, Woods Hole, MA 02543.].
- Baringer M. O., and J. Price, 1997a: Mixing and spreading of the Mediterranean outflow. *J. Phys. Oceanogr.*, **27**, 1654–1677. [Find this article online](#)
- Baringer M. O., and J. Price, 1997b: Momentum and energy balance of the Mediterranean outflow. *J. Phys. Oceanogr.*, **27**, 1678–1692. [Find this article online](#)
- Blanke B., and P. Delecluse, 1993: Variability of the tropical Atlantic Ocean simulated by a general circulation model with two different mixed-layer physics. *J. Phys. Oceanogr.*, **23**, 1363–1388. [Find this article online](#)
- Bleck R., and D. Boudra, 1986: Wind driven spin-up in eddy-resolving ocean models formulated in isopycnic and isobaric coordinates. *J. Geophys. Res.*, **91**, 7611–7621.
- Bleck R., and L. Smith, 1990: A wind driven isopycnic coordinate model of the north and equatorial Atlantic Ocean. Model development and supporting experiments. *J. Geophys. Res.*, **95**, 3273–3285.
- Bleck R., C. Rooth, D. Hu, and L. Smith, 1992: Salinity-driven thermocline transients in a wind and thermohaline forced isopycnic coordinate model of the North Atlantic. *J. Phys. Oceanogr.*, **22**, 1486–1505. [Find this article online](#)
- Charney J. G., and M. Stern, 1962: On the instability of internal baroclinic jets in a rotating atmosphere. *J. Atmos. Sci.*, **19**, 159–172. [Find this article online](#)
- Chérubin L., X. Carton, and D. Dritschel, 1996: Vortex expulsion by a zonal transverse canyon. *Proc. of the Second Int. Workshop on Vortex Flows*, Paris, France, ESAIM Series, Société de Mathématiques Appliquées Industrielles, 101–121.
- Chérubin L., Coauthors, 1997: Descriptive analysis of the hydrology and currents on the Iberian shelf from Gibraltar to Cape Finisterre: Preliminary results from the SEMANE and INTERAFOS experiments. *Ann. Hydrogr.*, **21**, 5–69, (768). [Find this article online](#)
- Chérubin L., X. Carton, J. Paillet, Y. Morel, and A. Serpette, 2000: Instability of the Mediterranean water undercurrent southwest of Portugal: Effect of baroclinicity and topography. *Oceanol. Acta*, **23**(5), 551–573.
- Cushman-Roisin B., 1994: *Introduction to Geophysical Fluid Dynamics*. Prentice Hall, 320 pp.
- d'Asaro E., 1988: Generation of submesoscale vortices: A new mechanism. *J. Geophys. Res.*, **93**, 6685–6693.
- Ertel H., 1942: Ein neuer hydrodynamischer wirbelsatz. *Meteor. Z.*, **59**, 271–281. [Find this article online](#)
- Ferron B., H. Mercier, K. Speer, A. Garget, and K. Polzin, 1998: Mixing in the Romanche fracture zone. *J. Phys. Oceanogr.*, **28**, 1929–1945. [Find this article online](#)

- Fortuin J. M. H., 1960: Theory and application of two supplementary methods of constructing density gradient columns. *J. Polym. Sci*, **44**, 505–515.
- Hallberg R., 1999: Time integration of diapycnal diffusion and Richardson number dependent mixing in isopycnal coordinate ocean models. *Mon. Wea. Rev*, **128**, 1402–1419. [Find this article online](#)
- Haynes P., and M. McIntyre, 1987: On the evolution of vorticity and potential vorticity in the presence of diabatic heating and frictional or other forces. *J. Atmos. Sci*, **44**, 828–841. [Find this article online](#)
- Haynes P., and M. McIntyre, 1990: On the conservation and impermeability for potential vorticity. *J. Atmos. Sci*, **47**, 2021–2031. [Find this article online](#)
- Hogg N., and H. Stommel, 1985: The heton, an elementary interaction between discrete baroclinic geostrophic vortices, and its implications concerning eddy heat flow. *Proc. Roy. Soc. London Ser.*, **397A**, 1–20.
- Holopainen E., 1961: On the effect of friction in baroclinic waves. *Tellus*, **13**, 363–367. [Find this article online](#)
- Hoskins B., M. McIntyre, and W. Robertson, 1985: On the use and significance of isentropic potential vorticity maps. *Quart. J. Roy. Meteor. Soc.*, **111**, 877–946. [Find this article online](#)
- Howard L., 1961: Note on a paper of John W. Miles. *J. Fluid Mech*, **10**, 509–512. [Find this article online](#)
- Hu D., 1996: The computation of diapycnal diffusion and advective scalar fluxes in multilayer isopycnal-coordinate ocean models. *Mon. Wea. Rev*, **124**, 1834–1851. [Find this article online](#)
- Johnson G., T. Sanford, and M. O. Baringer, 1994: Stress on the Mediterranean outflow plume. Part I: Velocity and water property measurements. *J. Phys. Oceanogr*, **24**, 2072–2092. [Find this article online](#)
- Keyser D., and R. Rotunno, 1990: On the formation of potential vorticity anomalies in upper-level jet front systems. *Mon. Wea. Rev*, **118**, 1914–1921. [Find this article online](#)
- Klinger B., 1993: Gyre formation at a corner by rotating barotropic coastal flows along a slope. *Dyn. Atmos. Oceans*, **19**, 27–63. [Find this article online](#)
- Kushner P., 1995: A generalized Charney–Stern theorem for the semi-geostrophic dynamics. *Tellus*, **47**, 541–547. [Find this article online](#)
- Lamarque J. F., 1993: Analysis of mass transport and potential vorticity budget in a simulated tropopause folding. Ph.D. thesis, Catholic University of Louvain, Louvain-la-Neuve, Belgium, 199 pp.
- Lamarque J. F., and P. Hess, 1994: Cross-tropopause mass exchange and potential vorticity budget in a simulated tropopause folding. *J. Atmos. Sci*, **51**, 2246–2268. [Find this article online](#)
- Lampert L., 1998: Validation et traitement des données des flotteurs lagrangiens de type surdrift. Campagne SEMANE 97, SHOM Tech. Rep. 56/EPHOM/CMO/CM/NP, 39 pp. [Available from SHOM, BP 426, 29275 Brest Cedex, France.].
- Large W. G., J. C. McWilliams, and S. C. Doney, 1994: Oceanic vertical mixing: A review and a model with a nonlocal boundary layer parameterization. *Rev. Geophys*, **32**, 363–403. [Find this article online](#)
- Legg S., and J. Marshall, 1993: A heton model of the spreading phase of open-ocean deep convection. *J. Phys. Oceanogr*, **23**, 1040–1056. [Find this article online](#)
- Legg S., J. C. McWilliams, and J. Gao, 1998: Localization of deep ocean convection by a mesoscale eddy. *J. Phys. Oceanogr*, **28**, 944–970. [Find this article online](#)
- Marshall J., 1988: Submarine salt lenses. *Nature*, **333**, 594–595. [Find this article online](#)
- Mauritzen C., Y. Morel, and J. Paillet, 2001: Mediterranean water influence on the central waters of the North Atlantic. *Deep-Sea Res. I*, **48**, 347–381.
- McIntyre M., and W. Norton, 1990: Dissipative wave-mean interactions and the transport of vorticity or potential vorticity. *J. Fluid Mech*, **212**, 403–435. [Find this article online](#)
- McWilliams J. C., and P. R. Gent, 1980: Intermediate models of planetary circulations in the atmosphere and ocean. *J. Atmos. Sci*, **37**, 1657–1678. [Find this article online](#)
- Mied R. P., J. C. McWilliams, and G. J. Lindemann, 1991: The generation and evolution of mushroom-like vortices. *J. Phys. Oceanogr*, **21**,

Miles J. W., 1961: On the stability of heterogeneous shear flows. *J. Fluid Mech*, **10**, 496–508. [Find this article online](#)

Nof D., 1991: Lenses generated by intermittent currents. *Deep-Sea Res*, **38**, 325–345.

Pacanowski R., and S. Philander, 1981: Parameterization of vertical mixing in numerical models of tropical oceans. *J. Phys. Oceanogr*, **11**, 1443–1451. [Find this article online](#)

Paillet J., B. Le Cann, A. Serpette, Y. Morel, and X. Carton, 1999: Real-time tracking of a northern Meddy in 1997–1998. *Geophys. Res. Lett*, **26**, 1877–1880. [Find this article online](#)

Pedlosky J., 1987: *Geophysical Fluid Dynamics*. Springer, 710 pp.

Peters H., and M. C. Gregg, 1988: On the parameterization of equatorial turbulence. *J. Geophys. Res*, **93**, 1199–1218.

Pichevin T., and D. Nof, 1996: The eddy canon. *Deep-Sea Res*, **43**, 1475–1507.

Pingree R., 1994: Winter warming in the southern Bay of Biscay and Lagrangian eddy kinematics from a deep-drogued Argos buoy. *J. Mar. Biol. Assoc. U.K*, **74**, 107–128. [Find this article online](#)

Pingree R., and B. Le Cann, 1992a: Three anticyclonic slope water oceanic eddies (SWODDIES) in the southern Bay of Biscay in 1990. *Deep-Sea Res*, **39**, 1147–1175.

Pingree R., and B. Le Cann, 1992b: Anticyclonic eddy X91 in the southern Bay of Biscay, May 1991 to February 1992. *J. Geophys. Res*, **97**, 14 353–14 367.

Pingree R., and B. Le Cann, 1993: A shallow Meddy (a SMEDDY) from the secondary Mediterranean salinity maximum. *J. Geophys. Res*, **98**, 20 169–20 185.

Prater M., 1992: Observations and hypothesized generation of a Meddy in the Gulf of Cadiz. Applied Physics Laboratory, University of Washington, Tech. Rep. APL-UW TR9210, 143 pp. [Available from Applied Physics Laboratory, University of Washington, 1013 NE 40th Street, Seattle, WA 98105.]

Price J., and M. O. Baringer, 1994: Outflows and deep water production by marginal seas. *Progress in Oceanography*, Vol. 33, Pergamon, 161–200.

Rhein M., and H. Hinrichsen, 1993: Modification of the Mediterranean water in the Gulf of Cadiz, studied with hydrographic, nutrient and chlorofluoromethane. *Deep-Sea Res*, **40**, 267–291.

Ripa P., 1991: General stability conditions for a multi-layer model. *J. Fluid Mech*, **222**, 119–137. [Find this article online](#)

Rivière P., 1995: Effets de la friction sur l'instabilité barocline. Thèse de doctorat de l'Université de Bretagne Occidentale, Brest, France, 169 pp.

Rivière P., and P. Klein, 1997: Effects of asymmetric friction on the nonlinear equilibration of a baroclinic system. *J. Atmos. Sci*, **54**, 1610–1627. [Find this article online](#)

Rossby C., 1939: Relation between variations in the intensity of the zonal circulation of the atmosphere and the displacements of the semi-permanent centers of action. *J. Mar. Res*, **2**, 38–55. [Find this article online](#)

Shen C., and T. Evans, 1994: On vorticity shedding by unstable jets. *Dyn. Atmos. Oceans*, **21**, 105–135. [Find this article online](#)

Smagorinsky J. S., 1963: General circulation experiments with the primitive equations. I. The basic experiment. *Mon. Wea. Rev*, **91**, 99–164. [Find this article online](#)

Spall M., and J. Price, 1998: Mesoscale variability in Denmark Strait: The PV outflow hypothesis. *J. Phys. Oceanogr*, **28**, 1598–1623. [Find this article online](#)

Stern M., and J. Whitehead, 1990: Separation of a boundary jet in a rotating fluid. *J. Fluid Mech*, **217**, 41–69. [Find this article online](#)

Valdivieso da Costa M., 1999: Numerical simulations of boundary currents of intermediate density in comparison with laboratory experiments: Eddy formation and transport. Ph.D. dissertation, Laboratoire d'Océanographie Physique, Université de Bretagne Occidentale, 215 pp. [Available from Laboratoire d'Océanographie Physique, Université Bretagne Occidentale, BP 809, 29285 Brest Cedex, France.]

6. PV Inversion

Under the assumption of geostrophic balance, the PVA profile specified in (14) can be inverted to calculate both the corresponding velocity and layer depths. However, because the PVA is a nonlinear combination of the latter fields, an iterative procedure has to be developed. We summarize it below.

Given a PVA field, the inversion equations can be written

$$\begin{aligned} \frac{H_k}{h_k} \left(\zeta_k - f \frac{\Delta h_k}{H_k} \right) &= \Delta Q_k \\ f \zeta_k &= \nabla^2 M_k \\ M_k &= \sum_{i=1}^{i=k-1} \frac{\rho_i}{\rho_k} g \Delta h_i + \sum_{i=k}^{i=N} g \Delta h_i. \end{aligned} \quad (\text{A1})$$

The first equation in (A1) can thus be expressed in term of the layer thickness anomalies $(\Delta h_1, \dots, \Delta h_N)$, and the iterative procedure we chose to solve (A1) is

$$\begin{aligned} \left(\zeta_k^{n+1} - f \frac{\Delta h_k^{n+1}}{H_k} \right) &= \Delta Q_k \left(1 + \frac{\Delta h_k^n}{H_k} \right) \\ f \zeta_k^{n+1} &= \nabla^2 M_k^{n+1} \\ M_k^{n+1} &= \sum_{i=1}^{i=k-1} \frac{\rho_i}{\rho_k} g \Delta h_i^{n+1} + \sum_{i=k}^{i=N} g \Delta h_i^{n+1} \\ h_k^0 &= 0. \end{aligned} \quad (\text{A2})$$

Iterations are stopped when $\max_k (|h_k^{n+1} - h_k^n|) \leq \epsilon$ (where we have chosen $\epsilon = 10^{-3}$ m).

It is worth noting that the system (A2) is equivalent to a quasigeostrophic PV inversion (except for the right-hand side of the first equation), for which solution methods are well known. After projection on the eigenmodes of the matrix linking M and Δh , the first equation becomes

$$\partial_y^2 \Delta h_k^{n+1} - \gamma_k^2 \Delta h_k^{n+1} = \text{RHS}_k^n, \quad (\text{A3})$$

where γ_k^2 is the eigenvalue associated to the k th eigenmode. The latter equation is easily solved analytically, given two boundary conditions. Boundary conditions are given by the constraint that the fluid is unperturbed away from the southern boundary, that is to say $\Delta h = 0$ and $\partial_y h = 0$ when $y \rightarrow \infty$. This entirely determines the solution for the barotropic part of the flow, when $\gamma = 0$, but for baroclinic modes ($\gamma \neq 0$) the two previous constraints are equivalent, and there exists a degree of freedom that can be used, for instance, to chose Δh_k or $\partial_y h_k$ at the coast. This is what is done here: we specify the vertical profile of the velocity field at the coast. In the case presented in this paper, the latter corresponds to the first baroclinic mode with a maximum speed of 0.8 m s^{-1} . This yields a minimum Richardson number of about 1 for the flow.

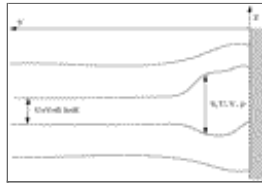
Tables

TABLE 1. Isopycnal and diapycnal mixing coefficients used in experiments given in Fig. 7

Expt	K_∞	ν_0	C_s
a	$0 \text{ cm}^2 \text{ s}^{-1}$	$0 \text{ m}^2 \text{ s}^{-1}$	0
b	$0 \text{ cm}^2 \text{ s}^{-1}$	$1 \text{ m}^2 \text{ s}^{-1}$	0.005
c	$500 \text{ cm}^2 \text{ s}^{-1}$	$1 \text{ m}^2 \text{ s}^{-1}$	0.005
d	$0 \text{ cm}^2 \text{ s}^{-1}$	$20 \text{ m}^2 \text{ s}^{-1}$	0.005
e	$0 \text{ cm}^2 \text{ s}^{-1}$	$10^6 \text{ m}^2 \text{ s}^{-1}$	0

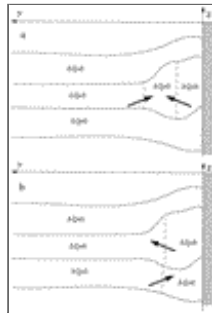
[Click on thumbnail for full-sized image.](#)

Figures



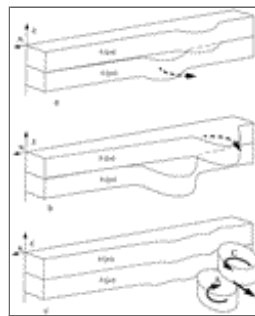
[Click on thumbnail for full-sized image.](#)

FIG. 1. The ocean is represented by a stably stratified sequence of homogeneous layers in which density and velocity are independent of depth. A layer is characterized by its horizontal velocity field (U , V), layer thickness h , and density, ρ . Far from the boundary, the fluid is at rest



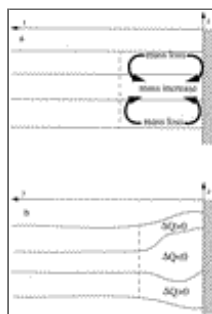
[Click on thumbnail for full-sized image.](#)

FIG. 2. Two different PVA distributions that satisfy the C–S necessary condition for instability: (a) the PVA gradient changes sign within a layer and (b) the PVA gradient changes sign at different depths. The arrows represent the PV gradient for the given distribution



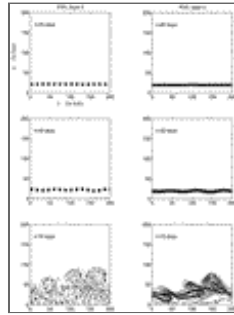
[Click on thumbnail for full-sized image.](#)

FIG. 3. Schematic evolution of the PVA distribution of a current that satisfies the C–S criterion for instability because its PVA gradient changes sign with depth. Baroclinic instability leads to the formation and detachment of a baroclinic dipole (heton)



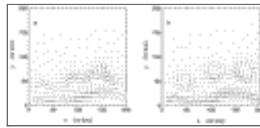
[Click on thumbnail for full-sized image.](#)

FIG. 4. A thought experiment illustrating the H–M constraint: (a) a resting ocean with uniform PV in each layer is mixed diapycnally so that (b) the layer gaining mass during the mixing process develops a negative PVA and the layers losing mass positive ones



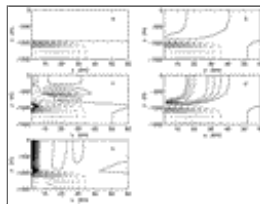
Click on thumbnail for full-sized image.

FIG. 5. PVA evolution in density layers 3 (left column) and 4 (right column), with the positive (negative) contours drawn as solid (dashed) lines. Starting from rest at $t = 0$ (not shown), the water column is mixed, and a finite PVA develops in each layer. Mixing near the southern boundary leads to a current profile that is baroclinically unstable, and baroclinic dipoles emerge after about 60 days



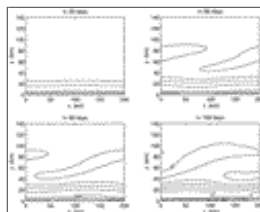
Click on thumbnail for full-sized image.

FIG. 6. Velocity field in layers (a) 4 and (b) 3 at a time 70 days after the mixing began



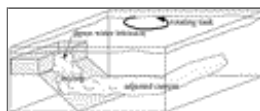
Click on thumbnail for full-sized image.

FIG. 7. PVA distributions in 2D integrations after 10 days for different isopycnal and diapycnal mixing parameters given in [Table 1](#). Positive contours are solid lines, and negative ones are dashed. The contour interval is $0.025f$. Notice the development of positive PVA for diapycnal mixing (c) and strong isopycnal mixing (d and e)



Click on thumbnail for full-sized image.

FIG. 8. PVA in 3D integrations in the upper layer at time $t = 50, 80, 90, 100$ days [respectively (a), (b), (c), and (d)]. A positive PVA has rapidly developed and meanders grow after about 80 days. At $t = 100$ days, small-scale noise appears because of the use of weak isopycnal diffusion, and the computation has to be either stopped or resumed with higher viscosity



Click on thumbnail for full-sized image.

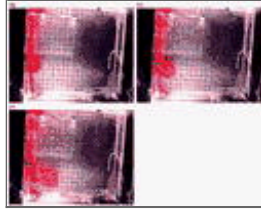
FIG. 9. Experimental setup for the rotating-tank experiment





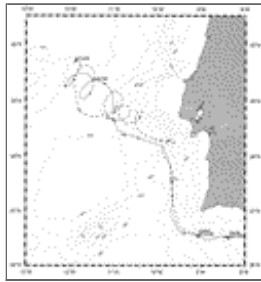
[Click on thumbnail for full-sized image.](#)

FIG. 10. Photographic side view of the rotating-tank experiment. The intermediate current is visualized by red fluid. Dye grains are dropped to create vertical streaks that indicate the velocity vertical profile by their horizontal displacements. The current is strongest at middepth. Vertical motions are weak, indicating a geostrophic balance



[Click on thumbnail for full-sized image.](#)

FIG. 11. Photographic top view of the rotating-tank experiment. A meander develops on the intermediate current near the left wall of the tank (a). Two “days” later (1 day = 1 table turnover time = 20 s) it grows and emerges as a baroclinic dipole, with its characteristic mushroom shape (b), which eventually detaches from the boundary current (c) four days later



[Click on thumbnail for full-sized image.](#)

FIG. 12. Trajectories of two floats released at 1000 and 1300 m (dashed and plain lines, respectively) off of the Iberian coast. Note the anticyclonic loops of the shallower float, typical of a parcel trapped in a meddy, and the cyclonic loops of the deeper float

¹ In the H–M papers, the conserved integral has a mass-weighted integrand. The volume-weighted result here is equivalent when the Boussinesq approximation is made, as is appropriate for the ocean.

Corresponding author address: Dr. Yves Morel, EPSHOM-CMO, B.P. 426, Brest Cedex 29275, France. E-mail: morel@shom.fr

[top ▲](#)



© 2008 American Meteorological Society [Privacy Policy and Disclaimer](#)

Headquarters: 45 Beacon Street Boston, MA 02108-3693

DC Office: 1120 G Street, NW, Suite 800 Washington DC, 20005-3826

amsinfo@ametsoc.org Phone: 617-227-2425 Fax: 617-742-8718

[Allen Press, Inc.](#) assists in the online publication of AMS journals.